

Title	Multiple Coincident Eruptive Seismic Tremor Sources During the 2014-2015 Eruption at Holuhraun, Iceland
Creators	Eibl, Eva P. S. and Bean, Christopher J. and Jónsdóttir, Ingibjoerg and Höskuldsson, Armann and Thordarson, Thorvaldur and Coppola, Diego and Witt, Tanja and Walter, Thomas
Date	2017
Citation	Eibl, Eva P. S. and Bean, Christopher J. and Jónsdóttir, Ingibjoerg and Höskuldsson, Armann and Thordarson, Thorvaldur and Coppola, Diego and Witt, Tanja and Walter, Thomas (2017) Multiple Coincident Eruptive Seismic Tremor Sources During the 2014-2015 Eruption at Holuhraun, Iceland. Journal of Geophysical Research: Solid Earth, 122.
URL	https://dair.dias.ie/id/eprint/385/

please cite as: Eibl, E. P. S., Bean, C. J., Jónsdóttir, I., Höskuldsson, A., Thordarson, T., Coppola, D., Witt, T., Walter, T. R. (2017), Multiple Coincident Eruptive Seismic Tremor Sources During the 2014-2015 Eruption at Holuhraun, Iceland, *Journal of Geophysical Research: Solid Earth* 122, DOI: 10.1002/2016JB013892

Multiple Coincident Eruptive Seismic Tremor Sources During the 2014-2015 Eruption at Holuhraun, Iceland

Eva P. S. Eibl^{1,2}, Christopher J. Bean², Ingibjörg Jónsdóttir³, Armann Höskuldsson³, Thorvaldur Thordarson³, Diego Coppola⁴, Tanja Witt⁵, Thomas R. Walter⁵

¹School of Earth Sciences, University College Dublin, Belfield, Dublin 4, Ireland

²Geophysics Section, School of Cosmic Physics, Dublin Institute for Advanced Studies, 5 Merrion Square, Dublin 2, Ireland

³Institute of Earth Sciences, University of Iceland, Askja, Building of Natural Sciences, Sturlugata 7, 101 Reykjavík, Iceland

⁴Università di Torino, Dipartimento di Scienze della Terra, Turin, Italy

⁵GFZ - German Research Center for Geosciences, Potsdam, Germany

Key Points:

- Surprisingly, 3 tremor sources with different underlying mechanisms were detected in eruptive tremor during the Holuhraun eruption 2014/15.
- Tremor was generated (i) below open vents, (ii) at the margins of a growing lava flow field and (iii) potentially by intrusions at depth.
- Tremor sources need to be accurately selected and located for quantification of effusion rates for example, if multiple sources are present.

Corresponding author: Eva P. S. Eibl, eva.ps.eibl@hotmail.com

Abstract

We analyze eruptive tremor during one of the largest effusive eruptions in historical times in Iceland (2014/15 Holuhraun eruption). Seismic array recordings are compared with effusion rates deduced from MODerate resolution Imaging Spectroradiometer (MODIS) recordings and ground video monitoring data and lead to the identification of three coexisting eruptive tremor sources. This contrasts other tremor studies that generally link eruptive tremor to only one source usually associated with the vent. The three sources are (i) a source that is stable in back azimuth and shows bursts with ramp-like decrease in amplitude at the beginning of the eruption. We link it to a process below the open vents where the bursts correlate with the opening of new vents and temporary increases in the lava fountaining height. (ii) a source moving by a few degrees per month while the tremor amplitude suddenly increases and decreases. Back azimuth and slowness correlate with the growing margins of the lava flow field whilst contact with a river led to fast increases of the tremor amplitude. (iii) a source moving by up to 25° southwards in 4 days that cannot be related to any observed surface activity and might be linked to intrusions. We therefore suggest that eruptive tremor amplitudes/ energies are used with caution when estimating eruptive volumes, effusion rates or the eruption explosivity as multiple sources can coexist during the eruption phase. Our results suggest that arrays can monitor both the growth of a lava flow field and the activity in the vents.

1 Introduction

Volcano monitoring commonly includes seismological records and allows the distinction between different types of signals that are characteristic of volcanoes. A long-lasting, emergent signal - tremor - is usually observed during eruptions [McNutt, 1992] and often starts and ends with the extrusion of magma [Battaglia *et al.*, 2005a; Soosalu *et al.*, 2005; Langer *et al.*, 2011]. However, the precise mechanism that generates eruptive tremor is poorly understood because of limited on-site observations and measurements of sufficient quality [Senyukov *et al.*, 2015; Langer *et al.*, 2011] and poor constraints on tremor locations especially at depth.

Published tremor source models can be broadly grouped into four different classes: (i) the normal modes of a linear oscillator with open or closed ends are excited (e.g. Chouet [1988]), (ii) fluid flow excites the conduit walls (e.g. Julian [1994]), (iii) evenly spaced pulses continuously repeat (e.g. Neuberg *et al.* [2000]; Hotovec *et al.* [2013]) and (iv) hydrothermal boiling (e.g. Leet [1988]; Cannata *et al.* [2010]).

As an attempt to find a possible tremor model, the tremor is usually correlated with other direct observations. For example a correlation between tremor amplitude and the height of lava fountains [Alparone, 2003; McNutt, 1987; Koyanagi *et al.*, 1987] has been attributed to a resonating source. Tremor generated by fluid flow was assumed when the tremor amplitude correlated with the gas content in the magma [Tárraga *et al.*, 2014], the constriction of the conduit [Tárraga *et al.*, 2014] or conduit geometry [Julian, 1994] or the intensity of the eruption [Tárraga *et al.*, 2014; Belousov *et al.*, 2015; Falsaperla *et al.*, 2005; Soosalu *et al.*, 2005; Langer *et al.*, 2011; Julian, 1994]. For correlations of the tremor amplitude and SO_2 emission rate [Palma *et al.*, 2008; Nadeau *et al.*, 2011] or with infrasonic pressure [Ripepe *et al.*, 2009] or correlations of tremor bursts and spattering episodes [Patrick *et al.*, 2011; Coppola *et al.*, 2005] the tremor source was related to boiling activity.

While correlations were established in the above mentioned cases, this was not always the case. Eaton *et al.* [1987] found evidence that tremor amplitude and fountain height did not correlate except for times when the fissure was forced open at the beginning of an eruption episode. Similarly, Aki and Koyanagi [1981] observed a high correlation between tremor and volume of erupted material merely at the beginning of an eruption. Subsequently, Aki and Koyanagi [1981] described that the tremor amplitude decreased while the amount of erupted material remained high. Such a lack

of correlation might be due to more than one simultaneously active tremor source, as *Battaglia et al.* [2005a] suggested at Piton de la Fournaise based on the tremor locations they derived using an amplitude based location method.

Other studies do not attempt to resolve the tremor source model, but focus more on forecasting/ monitoring eruptions. *McNutt* [1994] for example suggested the use of the tremor amplitude in order to estimate the size of an eruption and the amount of ash that will be ejected (see also *Bernard et al.* [2016]). This idea is supported by studies suggesting that the tremor amplitude or energy and the effusion rate are linked [*Koyanagi et al.*, 1987; *Battaglia et al.*, 2005b; *Falsaperla et al.*, 2005; *Coppola et al.*, 2009]. However, others like *Coppola et al.* [2009] and *Allard et al.* [2011] also find that high tremor amplitudes occur when the magma discharge is low ($< 0.3 \text{ m}^3/\text{s}$) and link this to a change in eruptive style.

Here we present the eruptive tremor that accompanied the 2014-2015 fissure eruption at Holuhraun, fed from Bárðarbunga volcano in Iceland [*Sigmundsson et al.*, 2014]. The tremor data were recorded with a seismic array at about 15 km distance from the fissure (Fig. 1) and compared to effusion rate estimates derived from MODIS sensor, lava fountain height measurements as derived from video records and the growing lava flow field.

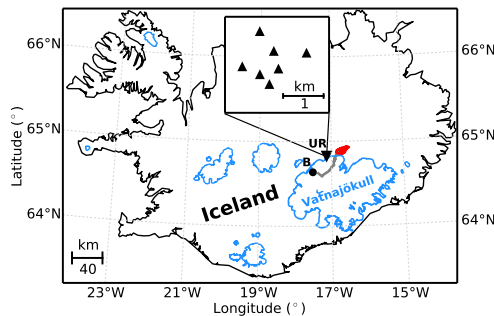


Figure 1. Geometry (inset) and location of seismometers arranged as a 7-element array UR northwest of Vatnajökull glacier, Iceland. Glaciers (blue), the 2014 formed dyke segments as described in *Sigmundsson et al.* [2014] (grey), the erupted lava flow field in Holuhraun (red) and Bárðarbunga volcano (B, black dot) are marked.

2 Overview of the Eruption

2.1 General Overview of the Fissures

From 16 August 2014 seismicity at 3 to 8 km depth propagated 48 km from beneath the ice covered Bárðarbunga volcano first towards the southeast, then north-northeast [*Sigmundsson et al.*, 2014]. At 0:02 UTC on 29 August a 4 hour long eruption started near the northern end of this migrating seismicity at Holuhraun - about 5 km north of the glacier's northern rim. On 31 August 2014 a fissure opened at the same place, with lava production that continued for 6 months until 27 February 2015. Additionally, a new fissure opened beneath the glacier on 3 September [*Eibl et al.*, 2017] and 2 km north of the ice on 5 September. The latter eruption was detected at 7:00 UTC by a news reporter and ended in the afternoon of 7 September. The vigour of the activity at the fissure from 5 to 7 September was much less than on the main vent system. A brief overview is given here of the evolution of the vent activity and the progressive growth of the lava flow field.

2.2 Vent Activity

The eruptions on 29 and 31 August began along a 600 m and 1.9 km long fissure, respectively [Hjartardóttir *et al.*, 2016]. They started with a continuous, aligned curtain of lava fountaining [Thordarson *et al.*, 2015] with higher activity on the southern and middle part of the fissure. On 1 September the activity on the fissure began to localize along specific vents. By 2 September the activity was concentrated on the vents named Nordri and Sudri located on the northern and southern end of the original fissure as well as the vents Heimasætan and Baugur situated along the middle segment of the original fissure (see Fig. 2 and 3). Within a few days, the ramparts of Heimasætan and Baugur merged into a single structure with at least 3 vents surrounded by an elongated rampart. We will refer to the middle part as Baugur hereafter. In the next few days Nordri, Sudri and Baugur built up ramparts. Nordri shut down between 11 and 12 September. No surface activity was seen from Sudri from 13 September (Fig. 2). Apart from two short-lived new vents Krakki (14 to 20/22 September) and an unnamed vent east to the fissure (14 to 16 September), the system stabilized from 22 September when Baugur was the only active part of the fissure with three feeding vents. From early February the lava level in Baugur dropped until the eruption stopped on 27 February 2015.

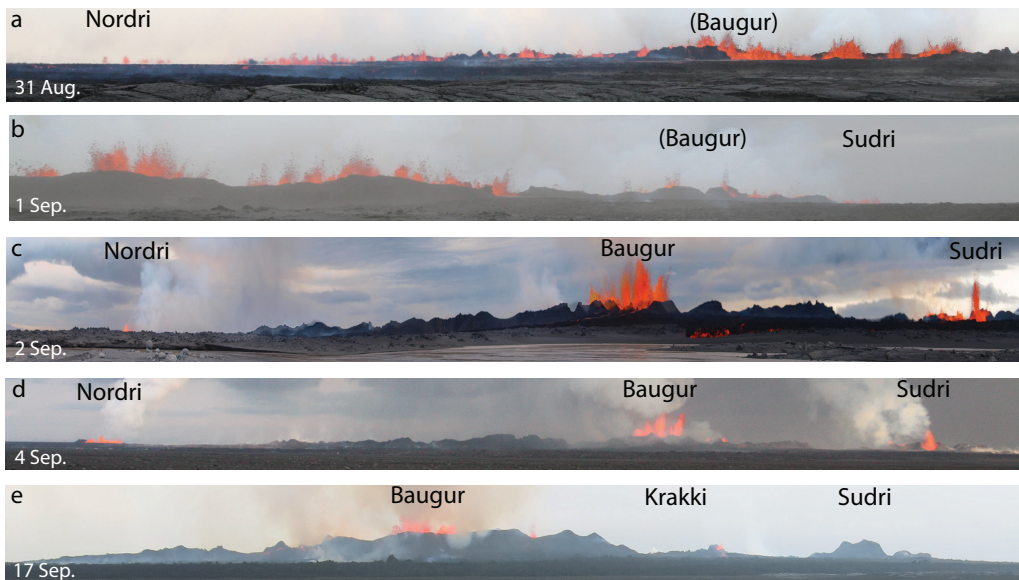


Figure 2. Vent activity along the fissure viewed from the west between 31 August and 17 September 2014. For an overview of vent locations and geometries see Fig. 3. (a) On 31 August the activity is continuously visible along the fissure. The southern end is not shown. Photo: Ármann Höskuldsson. (b) On 1 September the activity along the fissure started to focus. The northern end is not shown. Photo: Johanne Schmith. (c) On 2 September the activity focused on Nordri, Sudri and an elongated middle part consisting of Heimasætan and Baugur. Three feeding channels are visible in Baugur. Photo: Daniel Müller. (d) On 4 September the vent activity is as in c. Photo: Ármann Höskuldsson. (e) On 17 September merely Baugur and Krakki are active. Nordri and Sudri show no superficial activity. Photo: Águst Thór Gunnlaugsson.

2.3 Growth of the Lava Flow Field

The growth of the lava flow field (Fig. 3 and *Pedersen et al.* [2017]) was mapped in detail using GPS instruments in the field and data from satellites TERRA, AQUA, NOAA (daily), LANDSAT-8, LANDSAT-7, EO-1, SENTINEL-1, TerrasarX TandemX Radarsat2, Cosmo Skymed (weekly) and radar images from the Icelandic coastguard. The extruding basaltic lava initially flowed towards the northeast. It reached the river Jökulsá á Fjöllum on 7 September but continued northeastwards until 15 September (Fig. 3). Up until 26 September substantial lateral growth of the lava flow field took place both at the northwestern and southeastern margins. Thereafter, the growth was confined to the southeastern margins with minor activity in late October to mid November along the northern margins. New lava flows south of and parallel to the first one formed from 15 September, 22 September, 7 October, 12 October and 31 October.

The key elements of the flow field growth are (i) the lava transport system and (ii) the active flow fronts. While lateral growth of the flow field takes place at the active flow front, growth via inflation takes place within the lava flows and in particular over the internal pathways feeding lava to the active parts of the flow. When the eruption stopped on 27 February, 2015 the lava had covered an area of 85 km² and reached a height of 62 m in the vicinity of the fissure and an average lava thickness of 17 m [*Thordarson et al.*, 2015].

3 Methods

3.1 Frequency Wavenumber Analysis with Array Data

We installed an array (Fig. 1) from 30 August until 24 November 2014 in order to locate and track eruptive tremor sources spatially and temporally. An array is required as tremor does not have any clearly identifiable P and S wave arrivals but is recorded as coherent waveforms on different stations in the array. The array initially consisted of seven 3-component Guralp 6TDs (30 s to 100 Hz), of which four were replaced by Guralp 3ESPCD (60 s to 50 Hz) on 26 September. From late November only one station in the array continued to record. The array had an aperture of 1.63 km, a minimum station distance of 360 m, no angular dependence and was designed to resolve frequencies between 0.4 and 6 Hz based on a typical P wave velocity in the volcanic zone in Iceland of 2.5 km/s [*Flóvenz and Gunnarsson*, 1991].

We subdivide the recording of the vertical component in one hour long, not overlapping time windows. We detrend, taper, instrument correct and downsample to a sampling frequency of 20 Hz. Then we perform a frequency-wavenumber (FK) analysis between 0.8 and 2.0 Hz with a moving time window of 20 periods (14.3 s) in length and 20% overlap as implemented in *Beyreuther et al.* [2010]; *Megies et al.* [2011].

The FK analysis performs a grid search in a horizontal slowness grid with, in our case, a limit of ± 1.0 s/km and a stepsize of a fourth of the width of the main lobe (0.02 s/km), chosen based on the array response function and the properties of our data. The result is a time series of absolute power, semblance and jointly inverted back azimuth and slowness. We require a minimum semblance of 0.25 and use the time series of the back azimuth to create histograms with 0.8° wide bins. The dominant back azimuth is picked automatically and the median slowness calculated. By calculating histograms of the back azimuths we ensure that back azimuths from different sources are not averaged but that we pick the back azimuth associated with the dominating tremor source in each time window.

The back azimuth describes the angle between north and the direction towards the epicenter. The slowness is defined as the inverse of the apparent velocity of the wavefront and contains information about the wavetype and potentially the source-receiver distance. We estimate the error of each back azimuth and slowness value based on the shape and location of the main lobe of the array response function in

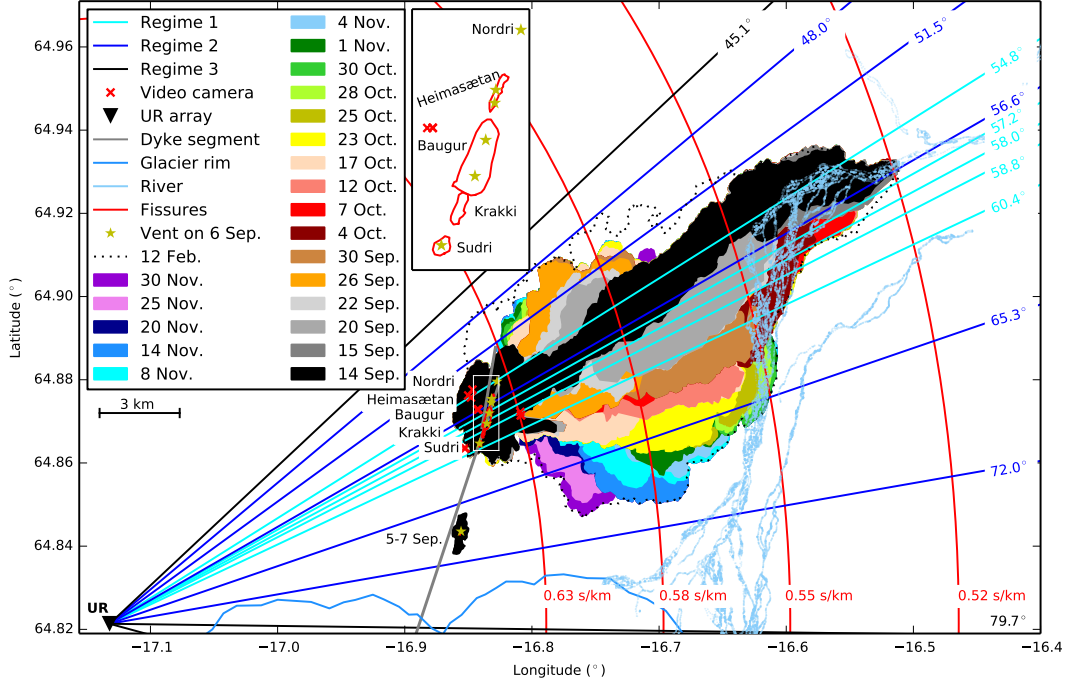


Figure 3. Growth of the lava flow field between 14 September and 30 November 2014. Lines mark the dyke segments as in *Sigmundsson et al.* [2014] (grey), the outline of Vatnajökull glacier (blue), Jökulsá á Fjöllum river (light blue) and the shape of the vents (red) as present in February i.e. Nordri, Heimasætan, Baugur, Krakki, Sudri and the fissures active during 5 to 7 September. Red crosses mark the location of the cameras used for lava fountain height calculation. Yellow stars mark the active vents on 6 September i.e. Nordri, Heimasætan (twice), Baugur (twice) and Sudri (see also inset). To ease comparison with Fig. 6 cyan, blue and black lines mark back azimuths with respect to seismic array UR. All back azimuths are corrected so that the 60.4° back azimuth aligns with Sudri (70.27°) (see text). Cyan lines mark the five back azimuths in Regime 1. Blue lines mark the minimum and maximum back azimuth in Regime 2 until 15 September, the southernmost one between 15 September and 21 October, the overall southern and the overall northern maximum. Black lines mark the minimum and maximum back azimuth observed for sources in Regime 3. Red circles mark locations on the surface with identical slownesses at UR. Slownesses given are based on a comparison of observed slownesses in Regime 2 and actively growing flow front at the same time (see Fig. 6d).

the horizontal slowness grid. We find all points with a power of at least 95% of the maximum, determine their corresponding slowness and back azimuth and calculate the standard deviation of these values [*La Rocca et al.*, 2008]. Our errors in back azimuth and slowness are 5.5 to 8° and 0.045 to 0.051 s/km, respectively.

3.2 Effusion Rate Derivation from Space-Based Thermal Data

MIROVA (Middle Infrared Observation of Volcanic Activity) is an automated global hot spot detection system run at the Università di Torino [*Coppola et al.*, 2016] based on near-real time ingestion of MODerate resolution Imaging Spectroradiometer (MODIS) data. The system completes automatic detection and location of high-temperature thermal anomalies and provides a quantification of the volcanic ra-

diant power (VRP) within 1 to 4 hours of each satellite overpass [Coppola *et al.*, 2016]. During the 2014/15 Holuhraun eruption, MIROVA provided a first-order indication of the ongoing effusive trend [Coppola *et al.*, 2017].

Satellite-based thermal data rely on the observed relationship between lava discharge rate, lava flow area and thermal flux (e.g. *Pieri and Baloga* [1986]; *Wright et al.* [2001]; *Harris* [2013] and references therein). For any given eruptive condition, this relationship allows VRP to be set as proportional to the time-averaged lava discharge rate (TADR), where the coefficient of proportionality ($c_{rad} = VRP/TADR$) takes into account the appropriate rheological, insulation and topographic conditions of the observed lava flow [Coppola *et al.*, 2013].

The best-fit coefficient ($c_{rad} \pm 50\%$) for the Holuhraun eruption has been calculated [Coppola *et al.*, 2017] on the basis of the silica content of the erupted lava as: $c_{rad} = 6.45 \cdot 10^{25} (X_{SiO_2})^{-10.4}$. By setting $X_{SiO_2} = 50.5$ wt% (http://earthice.hi.is/bardarbunga_2014) we obtain a radiant density of $0.6 - 1.8 \cdot 10^8$ J m⁻³ which is considered to incorporate the appropriate emplacement conditions for the lava flow. This range of values allowed us to provide a mean (Fig. 7b), upper and lower boundary limits for lava discharge rate calculation.

3.3 Lava Fountain Height Estimation from Video Records

Video recordings allow the monitoring of eruption sites and venting activity at high spatial and temporal resolution. In order to quantify changes in fountain height at the Holuhraun fissure during the first few days, we set up day-time video cameras recording the activity. The best locations (except on the first day of the eruption) were north-west of the fissure (see Fig. 3). Due to weather conditions, wind direction and the area covered by lava, the camera had to be moved slightly every day. Its distance was 0.5 to 2 km from the fissure and it had a field of view of 140 m x 80 m to 320 m x 180 m at the distance of the observed fissures. The length of the videos varied from several minutes up to 2 hours. The JVC GC-PX10 and Nikon D5100 cameras had a recording-frequency set to 50 frames/s and 25 frames/s, respectively. All videos were recording at a resolution of 1920 x 1080.

In order to calculate the height of the lava fountains in Baugur, Sudri and Nordri (see Fig. 3), we first convert each frame of a video into a grey scale image mainly based on the red channel of the camera. The red channel enabled us, for this particular case of fountaining, to better distinguish between lava, cloud and steam. Using a Sobel edge detection algorithm [Zhang *et al.*, 2009], we calculate the edges of the erupted lava fountain of each vent. All areas that are surrounded by strong edges are labeled by the regionsprops algorithm of MATLAB. The difference between the lowest pixel of all areas of one fountain and the highest pixel of the same fountain is the calculated height.

The videos are scaled by the distance to the lens and the lens type. Furthermore, we validated the resulting scaling by analysis of falling particles (assuming frictionless conditions) as in *Witt and Walter* [2017]. Due to different focal lenses and distances to the vents, the minimum size of detectable particles varied for every video, being in the range of 0.07 to 0.17m pixel size. To compare the different heights we only calculated heights of particles larger than ~ 20 cm. We give the error of the mean height as one standard deviation. The error of the maximum height is based on the accuracy of the edge detection (± 2 pixel unless the picture is very noisy) and the corresponding scaling from pixel to meter.

4 Results

The eruption was accompanied by harmonic, seismic tremor strongest between 0.7 and 1.5 Hz with overtones at a spacing of 0.1 Hz (Fig. 4). It was present throughout the whole eruption and with a constant frequency pattern.

The seismic array results (see Fig. 6b and c) indicate that the tremor came from a northeastern direction during our three month long record. Upon closer inspection of the back azimuth we subdivided the eruptive tremor into three regimes. Tremor in these three regimes had identical characteristics in the seismograms and spectrograms recorded at UR at 15 km distance. The regimes are active at the same time, are differentiated based on their source location and speed of source movement and are described in the following.

4.1 Correlation of the Vent Activity and Tremor Regime 1

The eruptive tremor started on 31 August at 4:14 UTC which we assume is the time when the fissure reopened. The open fissure was confirmed by recordings of a webcamera located on a hill 16 km northeast of the vents at 5:51 UTC when the fog had lifted.

In the time domain the tremor signal in Regime 1 shows five strong, 4 to 26 hours long pulses (Fig. 4a-d) during the first eight days of the eruption. The initial increase is sudden while the following decrease in amplitude is exponential. The first pulse can be linked to the opening of the fissure on 31 August, the fourth one to the opening of the southern fissures on 5 September. The third pulse is not further described here as it is associated with a pre-eruptive, shallowing tremor source beneath the glacier that is interpreted as the formation of a new dyke at less than 2 km depth [Eibl *et al.*, 2017] (see Table 1).

Camera monitoring of the fountain heights at the distinct vents suggests that the other two tremor bursts (see Fig. 4a-d) coincide with increases in fountain height. We observed a strong increase in lava fountain height at Baugur and Nordri from 31 August to 1 September (see Table 1) when the activity focused on fewer vents. At the same time the tremor amplitude decreased from the initial peak amplitude on 31 August (Fig. 5a) while parts of the fissure became inactive. The fountain height at Baugur and Nordri increased further on 2 September coinciding with an increase in tremor amplitude. Following a slight decrease in lava fountain height and tremor amplitude until 3 September, both increased on 4 September. The fountain height of Sudri seems to decrease between 31 August and 2 September. However, as the fountaining on 31 August is continuous, the fountain height in Sudri cannot be separated from Baugur.

Apart from an increase in tremor the opening of the southern fissures on 5 September is visible as an increase of back azimuth, a decrease in slowness (see Table 1) and higher frequency content between 1.3 and 1.8 Hz. Although these fissures remained active until 7 September, no tremor signal related to their activity was detected after 4:00 UTC on 6 September primarily because of more intense activity in the northern fissure. However, the tremor indicates that the fissures opened around 4:20 UTC on 5 September, 2 hours and 40 minutes before it was detected by a news reporter.

The back azimuth from UR array was - even in the first 24 h of the eruption - stable in the range of 54.8 to 60.4°. This is about 10° off the vents. In other studies a systematic offset between the actual source and array back azimuths was observed [Krüger and Weber, 1992; Schweitzer, 2001]. Reasons for this might be topographic features or heterogeneities in the bedrock that bend the seismic rays. In our case the systematic offset was stable in time and consistent for Regime 1 and 2 where the tremor location can be well constrained.

The tremor in Regime 1 (see Table 1) is characterized by five stable back azimuths (54.8, 57.2, 58.0, 58.8 and 60.4°) and slownesses in the range of 0.53 to 0.61 s/km (see Fig. 6b). We correct for array squinting by adding about 10° to the back azimuths and can align the back azimuths in Regime 1 with Nordri, the three lava fountains in Baugur and Sudri. This squint correction also aligns the back azimuths on 5/ 6 September with the eruption on 5 to 7 September.

The activity in the three main ramparts fits to the visibility of the back azimuths in Regime 1. This regime was the dominating tremor source until 15 September. The northern tremor source in Regime 1 became less visible shortly after Nordri stopped erupting in mid September. The lava fountain activity in Baugur slowed down to vigorous boiling with periodic bursting of bubbles in October while the three middle back azimuths were visible from time to time (see Fig. 6b). The highest lava fountains were in general associated with Baugur which is consistent with the fact that the middle three back azimuths dominated (Fig. 5b).

Apart from the above mentioned correlations between vent activity and tremor back azimuths in Regime 1, Sudri did not show any surface activity from mid September although the southernmost tremor source in Regime 1 continued to be active (see Fig. 6b). It is, however, possible that the tremor source after mid September was generated in the lava flow field as it points to a location where the feeding channels changed multiple times.

4.2 Correlation of the Lava Flow Field Growth and Tremor Regime 2

The tremor back azimuths in Regime 2 (see Table 2) gradually changed a few degrees southwards per month (see Fig. 6c). This regime dominated from 15 September to 21 October and from 2 to 24 November. From mid September the back azimuth gradually changed from around 62.5° to 65.5° (southwards) while back azimuths from 2 November were in the range of 64 to 70° . We subdivided the back azimuths in Regime 2 with five blue lines (see Fig. 6c). These lines are also shown in Fig. 3 in order to ease comparison. It can be seen that the tremor back azimuths correlate with the growth of the lava flow field. For example from 15 September when the back azimuths indicate a gradual southwards movement (see Fig. 6c), lava flows were emplaced further and further south (Fig. 3).

Slownesses scattered over 0.05 s/km but increased on average from around 0.55 to 0.6 s/km between 11 and 25 September, decreased back to 0.55 s/km until 5 October and increased again to 0.6 s/km until 21 October. From 2 November slownesses ranged from 0.51 to 0.59 s/km (see Fig. 6d). These gradual changes in slowness correlate with changes in distance between the newly formed lava flow field and UR array (Fig. 6d). In September and October increasing slownesses coincided with decreases in distance whilst decreases in slowness coincided with increases in distance. As the tremor source moves away from UR, body waves travel through deeper regions, arrive at UR more steeply and therefore at lower slownesses. This correlation supports a tremor source at the growing margins of the lava flow field at the surface of the bedrock.

In the time domain fast increases in tremor amplitude in Regime 2 occurred on 7, 19, 27 and 29 September, decreases on 15, 20 and 28 September, 7 and 17 October (see Fig. 4e and f). On site observations show that new lava flows flowed into Jökulsá á Fjöllum river four times (see Fig. 3, Fig. 6a and Table 2 for the exact times). The first three contacts were accompanied by sudden increases and decreases in the tremor amplitude (see Fig. 6) without any change in slowness or back azimuth. The fourth contact cannot be seen as the tremor source in Regime 3 dominated. One decrease on 17 October could not be attributed to a source.

4.3 Regime 3: Back Azimuth Changes Up To 25° in 4 Days

Tremor from Regime 3 dominated from 21 October to 2 November and is characterized by back azimuths that changed up to 25° in 4 days (see Fig. 6c). There are two fast southwards movements from 21 to 25 October (65 to 90°) and from 26 October to 2 November (45 to 74°). These movements correspond to a minimum horizontal movement (at the distance of the fissure) of about 10 km.

The corresponding slownesses gradually decrease from 0.58 to 0.48 s/km and 0.70 to 0.51 s/km, respectively (Fig. 6d). Decreasing slownesses indicate that the

Table 1. Comparison of back azimuths in Regime 1 with the active vents and times of tremor bursts with lava fountain height and opening fissures^a.

Date (Time) (UTC)	Tremor amplitude	Back azi- muth (°)	Slowness (s/km)	Mean fountain height (m) (max. fountain height)	Tremor Source in Regime 1
31 Aug. - 16 Sep.		54.8			Nordri
31 Aug. - 26 Nov.		57.2			Baugur
31 Aug. - 22 Nov.		58.0			Baugur
1 Sep. - 20 Nov.		58.8			Baugur
31 Aug. - 26 Sep.		60.4			Sudri
31 Aug. (4:14- 9:00)	Peak, exp. decrease	57.2	0.59-0.63	N: 6.9±2.4 (15.0±0.2) B/S: 46.5±6.6 (91.5±0.4)	New fissure opened
”	”	”	”		”
1 Sep.	Low			B: 64.1±12.4 (91.5±0.3) N: 48.7±5.7 (84.8±0.4)	-
”					”
2 Sep. (2:00-20:00)	Peak, exp. decrease	57.2	0.56-0.63	B: 92.2±6.9 (105.7±0.5)	Higher lava fountains
”	”	”	”	N: 62.9±10.8 (108.9±0.6)	”
”	”	”	”	S: 28.7±7.1 (69.8±0.6)	”
3 Sep. (2:00-21:35)	Three peaks	119-134	0.57-0.75	B: 96.9±13.3 (109.2±0.2)	Shallow dyke formed subglacially
”	”	”	”		[Eibl <i>et al.</i> , 2017]
”	”	”	”		
4 Sep.(6:03-22:00)	Peak, exp. decrease	57.2	0.53-0.60	B: 126.4±4.2 (133.0±0.7)	Higher lava fountains
5 Sep. (4:20) - 6 Sep. (6:00)	Two peaks	63-71	0.48-0.55		New fissure opened
”	”	”	”		2 km north of the ice

^aN, B and S denote Nordri, Baugur and Sudri, respectively.

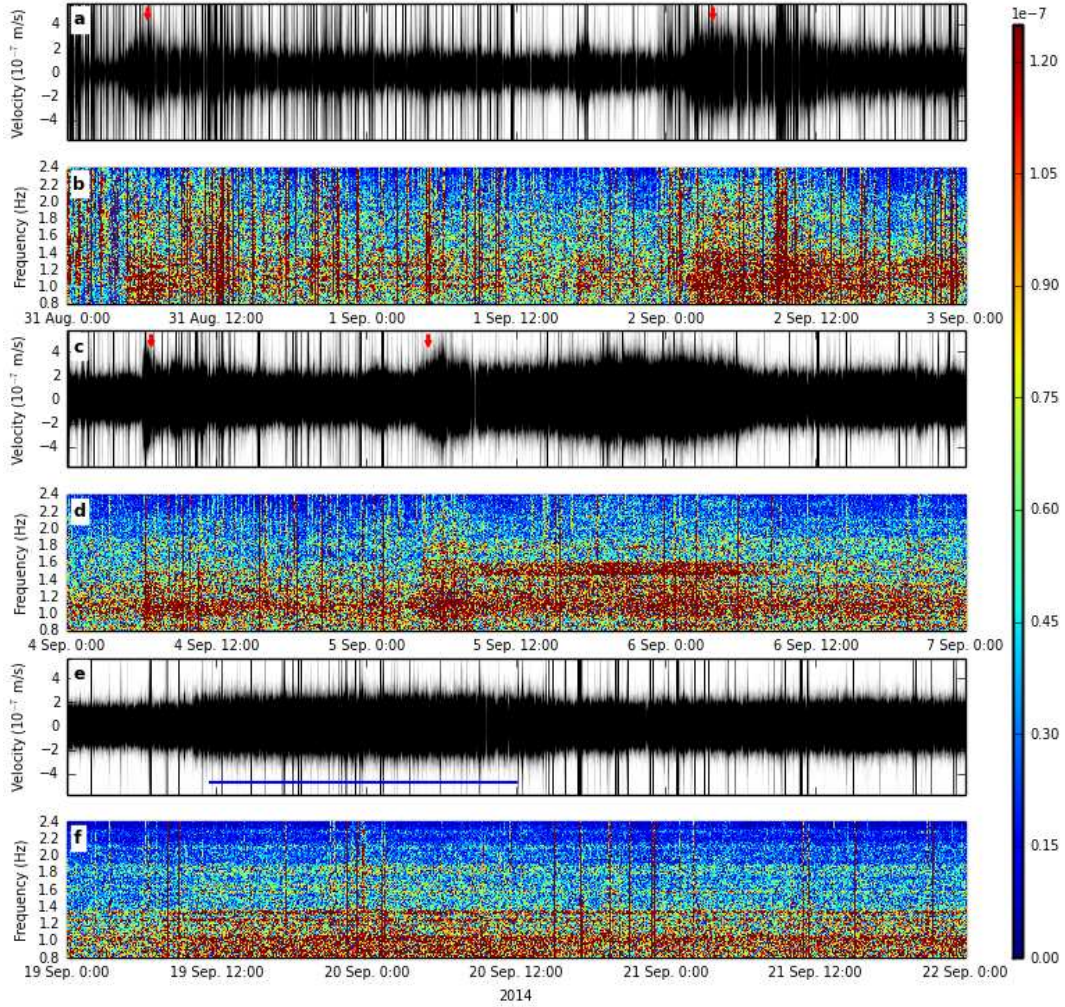


Figure 4. Instrument corrected seismogram and amplitude spectrogram of the eruptive tremor at UR array filtered between 0.8 and 2.4 Hz. The earthquakes appearing as vertical lines are mostly from the dyke and the continuing Bárðarbunga caldera collapse. We show all four tremor bursts in Regime 1 (red arrows) from (a & b) 31 August to 3 September and (c & d) 4 to 7 September. (e & f) One exemplary sudden increase and decrease in tremor amplitude in Regime 2 between 19 and 22 September is shown while the visually verified lava contact with the river is marked with a blue horizontal line.

tremor source either moved away from UR or that it is composed of more body waves. Consequently we assume that the tremor source either deepened in time or moved at the same depth laterally towards the southeast away from the vents (and UR array). A combination of both is also possible.

No change in tremor amplitude is visible at that time.

4.4 Correlation of Effusion Rate and Tremor Amplitude

The array - installed on 30 August - detected harmonic tremor from 4:14 UTC on 31 August until about 24 February. Apart from four peaks in the tremor within the first 8 days and erratic sudden increases or decreases, the tremor amplitude decreased

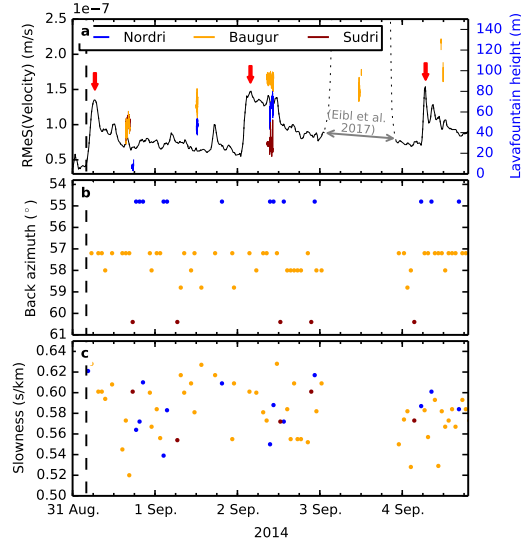


Figure 5. Tremor amplitude in comparison to the lava fountain height from 31 August to 5 September 2014. (a) The black line shows the tremor Root Median Square (RMeS) of the vertical component of station URB filtered between 0.8 and 2.0 Hz. Red arrows as in Fig. 4. The vertical, black, dashed line marks the start of the eruption. The RMeS on 3 September is dotted and truncated as this is shown and interpreted in *Eibl et al. [2017]*. The blue, orange and dark red lines show the lava fountain height in Nordri, Baugur and Sudri, respectively. (b) Colored dots mark each 1 h long time window where one of the five stable back azimuths in Regime 1 is dominating. Dots are colored according to the vents in a. (c) Same as in subfigure b but showing the associated slownesses.

gradually with time with occasional increases or decreases in amplitude. However, on 2 February the tremor amplitude increased and only reached the detection threshold of our array at 15 km distance from the fissures about three days before the eruption was officially declared over.

A general decrease in both effusion rate derived from satellites and tremor amplitude over 6 months can be observed (Fig. 7). On a smaller scale the effusion rate peaked from 7 to 11 September and around 5 October whilst the tremor amplitude was highest on 31 August to 5 September and 2 October. Excluding the increases and decreases in tremor amplitude, for example on 29 September, which are due to the contact with the river, the peak in tremor amplitude on 2 October is not as prominent as the peak in effusion rate. The offset between the MODIS-derived effusion rates and the tremor amplitude during sources in Regime 1 might be due to the fact that the satellite-based effusion rates assume the lava flow has reached a steady-state thermal state [*Garel et al., 2012*]. In basaltic flows this generally takes a few hours to a few days so that sharp variations in the lava flux are not immediately reflected by sharp variation of the radiant output.

In contrast, lows in effusion rate and tremor amplitude broadly coincide in mid September and mid October. From then on small scale fluctuations of tremor amplitude and effusion rate do not seem to correlate. However, the tremor increase by a factor of three in February roughly coincided with the deviation of the effusion rate from an exponential decreasing trend on 27 January [*Coppola et al., 2017*] and was also observed by *Allard et al. [2011]* on Piton de la Fournaise. A lack of correlation might be due to multiple coincident tremor sources or a dominant tremor source not related to processes in the vents.

Table 2. Comparison of back azimuths and slownesses in Regime 2 with the growing lava flow field and times of sudden increases and decreases in tremor amplitude with the contact with the river^a.

Date (Time in UTC)	Tremor amplitude	Back azimuth (°)	Slowness (s/km)	Features of the growth of the lava flow field (Regime 2)
11 Sep. - 25 Sep.		62.5→	0.55→0.6	flow field grows towards UR
25 Sep. - 5 Oct.		...	0.6→0.55	flow field grows away from UR
5 Oct. - 21 Oct.		→65.5	0.55→0.6	flow field grows towards UR
2 Nov. - 15 Nov.		64 - 70	0.51 - 0.59	
7 Sep. (18:20)	Increase			River reached
15 Sep. (3:20)	Decrease	64	0.55±0.02	River left
19 Sep. (10:55)	Increase	63	0.59±0.04	River reached
20 Sep. (16:30)	Decrease	63	0.58±0.03	River left
27 Sep. (8:35)	Increase	63.8	0.57±0.02	First snow
28 Sep. (8:35)	Decrease	63.8	0.57±0.02	
29 Sep. (10:05)	Increase	63.8	0.57±0.03	River reached
7 Oct. (11:45)	Decrease	64.2	0.56±0.04	River left
17 Oct. (12:25)	Decrease	64.2	0.58±0.03	

^aArrows indicate gradual movements in back azimuth or slowness.

5 Discussion

Eruptive tremor is usually interpreted to be associated with only one source in the literature. In contrast, we found three coexisting tremor sources in the eruptive tremor during a well-recorded eruption in Iceland. Below we discuss possible tremor generation models and implications for studies that use the tremor amplitude or energy to estimate input parameters for other models for example plume height models.

5.1 Regime 1: Vent Tremor Model

We summarize our observations regarding tremor Regime 1 below in order to find a possible vent tremor model:

(i) The eruptive tremor started/ ended with the opening/ closing of the fissure (see Fig. 7c).

(ii) Tremor was very narrowbanded, harmonic ($\Delta f=0.1$ Hz) and strongest from 0.7 to 1.5 Hz (see Fig. 4).

(iii) There were no frequency glidings or frequency jumps during these 6 months of eruption (see Fig. 4).

(iv) The vents (especially Baugur) had a temporary lava pond on top, that exhibited lava fountaining and spattering over the rampart.

(v) The tremor was generated locally below open vents, not while magma flowed horizontally in the 48 km long dyke (see Fig. 3).

(vi) Although a 1.9 km long fissure opened on the first day, the tremor source was already focused on certain directions where Nordri, Sudri and Baugur formed subsequently (see Fig. 6b).

(vii) Tremor was stronger when a new vent opened and lava fountains were higher (see Fig. 5a).

(viii) In the first few days of the eruption there were peaks in the tremor amplitude as well as in the effusion rate (see Fig. 7b and c).

(ix) Comparing the slownesses with the slownesses on 3 September [Eibl *et al.*, 2017], we suggest that the tremor source was at less than 2 km depths, but not on the surface.

Based on GPS and InSAR data (pers. comm. Andrew Hooper, December 2016) and mapping of superficial faults [Hjartardóttir *et al.*, 2016], the dyke was inferred to be as shallow as 300 m below the eruptive site on the day before the eruption. Tremor was from the very first day generated in 5 distinct regions presumably at a few hundred meters depth, above which vents formed later. Two scenarios regarding the evolution of the feeding system are possible:

(i) The dyke remained at about 300 m depth whilst magma was fed through 5 distinct 'fingers' to the surface. Three of these 'fingers' feed Baugur, whilst two feed Nordri and Sudri. The initial 1.9 km long fissure was fed sideways from these 'fingers' reflecting merely the weakness of the crust, not the feeding system.

(ii) The whole dyke reached the surface visible as a 1.9 km long fissure. However, from day 2 merely regions with more or faster flow remained open whilst other parts of the dyke shut down. These 5 regions generated tremor beneath Baugur, Nordri and Sudri (illustrated in Fig. 8). The latter scenario seems more likely to us given that the dyke reached at least 300 m depth and that the lava fountains increase with the focusing on single vents on day 2.

As eruptive tremor started only once the fissure opened it might be related to degassing processes as suggested for example by Soosalu *et al.* [2005]. Ripepe and Gordeev [1999] proposed that the tremor is the result of a viscoelastic response of the magma to a sudden pressure drop that is generated when bubbles coalesce. As decompression dominates over diffusion in the uppermost few hundred meters of the dyke, bubble growth speeds up. They propose that tremor is generated in a region merely 100 to 200 m beneath the surface. Based on a clear correlation between eruption type (effusive - Strombolian - lava fountain - sustained column) and tremor amplitude (increasing) Alparone [2003] suggested similarly that the tremor is generated at shallow depth. They observed systematic depth changes of the tremor source and link it to rising magma that starts to fragment and allows gas bubbles to coalesce and migrate.

An alternative model might be flow in the conduit as favored by Hibert *et al.* [2015] when they found a correlation between extrusion rate and tremor energy but no correlation with the infrasonic signal. However, as there were no infrasonic recordings in early September when the tremor in Regime 1 dominated we cannot comment on the applicability here.

5.2 Regime 2: Lava Flow Field Tremor Model

We summarize our observations in tremor Regime 2 in order to discuss sources related to the lava flow field:

(i) The tremor amplitude increased when lava was in contact with water from the river Jökulsá á Fjöllum (see Fig. 6a).

(ii) Although the lava flow field inflated and lava flowed in open or roofed channels, the tremor back azimuth (see Fig. 6c) and slowness (see Fig. 6d) correlated with the growing margins of the lava flow field (see Fig. 3).

(iii) Tremor was very narrowbanded, harmonic ($\Delta f=0.1$ Hz) and strongest from 0.7 to 1.5 Hz (see Fig. 4).

The observed correlations indicate that the tremor in Regime 2 was generated at the surface of the bedrock (Fig. 8). As changes in height were less than 60 m at a distance of 15 km to 30 km from UR array, changes in slowness were mainly caused by horizontal changes in distance as visible in Fig. 6d.

If the hot lava comes in sudden contact with cold water from the river, the water beneath the flow is converted into steam. This hydrothermal boiling is a viable tremor source as observed for example at Old Faithful Geyser [Kedar *et al.*, 1998]. However at Old Faithful Geyser the associated tremor amplitude at 30 m distance was less than $2 \cdot 10^{-8}$ m/s. We therefore doubt that tremor from hydrothermal boiling could be recorded at more than 15 km distance.

Once the lava reaches the surface it forms a lava flow field that is mainly cooled by the contact with air, water and the ground. While lava is continuously fed into the lava flow field, it inflates until margins start to fail. This failure of newly formed visco-elastic crust creates repeated microcracks that might merge into low-frequency tremor. Tremor is generated on all surfaces of the lava flow field but, in contact with water the steam can migrate up through cooling cracks and enhance the cooling of the lava flow, therefore allowing larger microearthquakes and stronger tremor from the sides. Rock deformation in the form of regularly repeating earthquakes was observed as a possible source of tremor in Hotovec *et al.* [2013] and Eibl *et al.* [2017].

During other eruptions the appearance of a lavaflow was not seen to affect the tremor amplitude [Alparone, 2003]. Lavafloes were also observed at times when no change in the tremor amplitude occurred [Langer *et al.*, 2011; Battaglia *et al.*, 2005a] or when tremor amplitude was low [Soosaku *et al.*, 2005]. Here, we similarly observed no change in tremor amplitude at times when the array results suggest a change from vent related to lava flow field related tremor.

5.3 Regime 3: Dyke Intrusions

The dominating tremor source in Regime 3 showed two fast southward movements (see Fig. 6c and d). This tremor source dominated over the tremor from the vents and lava flow field although the overall tremor amplitude increased only slightly. The slownesses indicate that these fast southwards movements happened farther from UR array (slowness of 0.48-0.58 s/km) than the lava flow field related tremor in the month before (0.55-0.60 s/km).

As this tremor source moved about 10 km southwards in 4 days - much more than the extent of the lava flow field - we suggest that they might be related to processes in the subsurface such as further dyke formations (see Fig. 8). A tremor source at depth can also easily explain lower associated slownesses as it creates more body waves than a superficial tremor source. However, it seems unlikely to us that a shallow tremor source would move downwards. We therefore speculate that the tremor source moved laterally towards the southeast with a slight decrease in depth to explain the slowness pattern.

According to the back azimuths the dykes originated at different locations: at depth north of Nordri and in the region below Sudri (see Fig. 8). Oblique, curved, slightly widening faults, originating around Sudri trending towards the south, are visible up to 200 m south of the lavafield about 1 km east of Sudri (pers. comm. Ásta Rut Hjartardóttir, December 2016, grey star in the inset of Fig. 8). They might mark the location of these slightly deepening intrusions on the surface. It was observed that the seismic expression of shallow dyke intrusions at less than 2 km depth is tremor and need not necessarily generate high-frequency earthquakes [Eibl *et al.*, 2017]. However, InSAR data that could clearly detect deformation associated with the opening fissures on 31 August and 5 September do not show any sign of intrusions after September (pers. comm. Stéphanie Dumont, June 2016). Alternatively this tremor could be unrelated to the volcanic activity.

5.4 Possible Applications of the Tremor Amplitude

In the past the tremor amplitude/ energy was used to find a suitable tremor source model, to estimate the effusive rate [Battaglia *et al.*, 2005a; Hibert *et al.*, 2015],

erupted volume [Battaglia *et al.*, 2005a; Hibert *et al.*, 2015], to track changes in the degassing regime [Coppola *et al.*, 2009] or to predict the explosivity index and amount of ash [McNutt, 1994; Bernard *et al.*, 2016].

Studies that found a correlation between the tremor energy and effusion rate [Hibert *et al.*, 2015; Battaglia *et al.*, 2005b] favored a tremor source representing flow of magma in the conduit. However, correlation of tremor amplitude and effusion rate [Coppola *et al.*, 2009; Koyanagi *et al.*, 1987] suggest that the degassing is the main tremor source (for underlying assumptions see [Coppola *et al.*, 2009]). Coppola *et al.* [2009] also suggested that a lack of correlation between effusion rate and tremor amplitude reflects a change in the degassing regime. They suggest that changes between fast and slow flow regimes can be tracked by comparing effusion rate derived from MODIS sensors with tremor amplitude.

The three tremor sources during the Holuhraun eruption were active at the same time with similar frequency and time domain properties and similar slownesses and back azimuth ranges. We might expect a correlation between the tremor amplitude/energy linked to the vents (Regime 1) with explosivity, effusion rate or the eruptive volume as suggested above. However, we would not expect a correlation with the overall tremor amplitude due to the tremor generation at the margins of the lava flow field (Regime 2) and its dependence on contact with water. In our case we can not interpret the lack of correlation between effusion rate and tremor amplitude as a change in degassing regime as in Coppola *et al.* [2009].

6 Conclusions

We observed 6 month of continuous eruptive tremor during a basaltic fissure eruption that started and ceased with the opening/ closing of the vent. The eruptive tremor was harmonic, continuous, strongest between 0.7 and 1.5 Hz with no frequency changes. We used it to pinpoint the eruption starts to 4:14 UTC on 31 August and 4:20 UTC on 5 September 2014. Additionally, we identified three eruptive tremor sources which is exceptional: (i) below open vents, (ii) at the margins of the growing lava flow field and (iii) migrating at less than 2 km depth beneath the surface. We speculate that the eruptive tremor was linked (i) to bubble generation, (ii) repeating microearthquakes and (iii) to horizontal dyke formations. However, based on the spectral content of the three tremor sources, they cannot be separated.

We further note that even at the beginning of the eruption when a 1.9 km long fissure opened, the tremor focused in five regions where the vents formed later. This fast focusing from an elongated fissure to distinct vents was also visible in videos and photos of the lava fountaining.

Increases in tremor amplitude could be associated with different processes. Increases in vent-related tremor were associated with stronger lava fountaining activity and new opening vents. Increases in lava flow field-related tremor were associated with contact with water or snow. In order to get a first order estimate of, for example, the effusion rate, only tremor sources related to the vents should be considered. However, our results suggest that if satellite data are not available (clouds, low repeat times), the region is not accessible and the array is close enough, arrays can be used to monitor the growth of a lava flow field in addition to the activity in the vents.

Acknowledgments

The data were collected and analyzed within the framework of FutureVolc, which has received funding from the European Union's Seventh Programme for research, technological development and demonstration under grant agreement No 308377. We thank Bergur H. Bergsson and Heiko Buxel for technical support, Magnús H. Steinarsson and Aoife Braiden for support in the field and Andrew Hooper, Freysteinn Sigmundsson and Ásta Rut Hjartardóttir for feedback on the schematic illustration. We thank

Emmanuel Pagneux and Vincent Drouin for data. Seismic data are available via the website: '<http://futurevolc.vedur.is/>'. The array processing was performed using the freely available Python toolbox ObsPy.

References

- Aki, K., and R. Koyanagi (1981), Deep Volcanic Tremor and Magma Ascent Mechanism Under Kilauea, Hawaii, *J. Geophys. Res.*, *86*(B8), 7095–7109, doi:10.1029/JB086iB08p07095.
- Allard, P., A. La Spina, G. Tamburello, A. Aiuppa, A. Coquet, F. Brenguier, D. Coppola, A. Di Muro, M. R. Burton, and T. Staudacher (2011), First cross-correlated measurements of magma dynamics and degassing during a dyke eruption at Piton de la Fournaise hot spot volcano, Reunion Island, in *American Geophysical Union, Fall Meeting 2011*.
- Alparone, S. (2003), Relationship between tremor and volcanic activity during the Southeast Crater eruption on Mount Etna in early 2000, *Journal of Geophysical Research*, *108*(B5), 1–13, doi:10.1029/2002JB001866.
- Battaglia, J., K. Aki, and T. Staudacher (2005a), Location of tremor sources and estimation of lava output using tremor source amplitude on the Piton de la Fournaise volcano: 2. Estimation of lava output, *Journal of Volcanology and Geothermal Research*, *147*(3-4), 291–308, doi:10.1016/j.jvolgeores.2005.04.006.
- Battaglia, J., K. Aki, and T. Staudacher (2005b), Location of tremor sources and estimation of lava output using tremor source amplitude on the Piton de la Fournaise volcano: 2. Estimation of lava output, *Journal of Volcanology and Geothermal Research*, *147*(3-4), 291–308, doi:10.1016/j.jvolgeores.2005.04.006.
- Belousov, A., M. Belousova, B. Edwards, A. Volynets, and D. Melnikov (2015), Overview of the precursors and dynamics of the 2012-13 basaltic fissure eruption of Tolbachik Volcano, Kamchatka, Russia, *Journal of Volcanology and Geothermal Research*, *307*, 22–37, doi:10.1016/j.jvolgeores.2015.06.013.
- Bernard, B., J. Battaglia, A. Proaño, S. Hidalgo, F. Váscquez, S. Hernandez, and M. Ruiz (2016), Relationship between volcanic ash fallouts and seismic tremor: quantitative assessment of the 2015 eruptive period at Cotopaxi volcano, Ecuador, *Bulletin of Volcanology*, *78*(11), 80, doi:10.1007/s00445-016-1077-5.
- Beyreuther, M., R. Barsch, L. Krischer, T. Megies, Y. Behr, and J. Wassermann (2010), ObsPy: A Python Toolbox for Seismology, *Seismological Research Letters*, *81*(3), 530–533, doi:10.1785/gssrl.81.3.530.
- Cannata, A., G. Di Grazia, P. Montalto, F. Ferrari, G. Nunnari, D. Patanè, and E. Privitera (2010), New insights into banded tremor from the 2008-2009 Mount Etna eruption, *Journal of Geophysical Research: Solid Earth*, *115*(12), doi:10.1029/2009JB007120.
- Chouet, B. A. (1988), Resonance of a fluid-driven crack: Radiation properties and implications for the source of long-period events and harmonic tremor, *Journal of Geophysical Research*, *93*(B5), 4375, doi:10.1029/JB093iB05p04375.
- Coppola, D., T. Staudacher, and C. Cigolini (2005), The May-July 2003 eruption at Piton de la Fournaise (La Réunion): Volume, effusion rates, and emplacement mechanisms inferred from thermal imaging and Global Positioning System (GPS) survey, in *Kinematics and dynamics of lava flows*, edited by G. Manga, M., and Ventura, July 2003, pp. 103–124, Geological Society of America Special Paper 396, doi:10.1130/2005.2396(08).
- Coppola, D., D. Piscopo, T. Staudacher, and C. Cigolini (2009), Lava discharge rate and effusive pattern at Piton de la Fournaise from MODIS data, *Journal of Volcanology and Geothermal Research*, *184*(1-2), 174–192, doi:10.1016/j.jvolgeores.2008.11.031.

- Coppola, D., M. Laiolo, D. Piscopo, and C. Cigolini (2013), Rheological control on the radiant density of active lava flows and domes, *Journal of Volcanology and Geothermal Research*, *249*, 39–48, doi:10.1016/j.jvolgeores.2012.09.005.
- Coppola, D., M. Laiolo, C. Cigolini, D. Delle Donne, and M. Ripepe (2016), Enhanced volcanic hot-spot detection using MODIS IR data: results from the MIROVA system, in *Detecting, Modelling and Responding to Effusive Eruptions.*, vol. 426, edited by S. A. Harris, A. J. L., De Groeve, T., Garel, F.&Carn, pp. 181–205, Geological Society, London, Special Publications, doi:10.1144/SP426.5.
- Coppola, D., M. Ripepe, M. Laiolo, and C. Cigolini (2017), Modelling satellite-derived magma discharge to explain caldera collapse., *Geology*, *accepted*, doi:10.1130/G38866.1.
- Eaton, J. P., D. H. Richter, and H. L. Krivoy (1987), Cycling of magma between the summit reservoir and Kilauea Iki lava lake during the 1959 eruption of Kilauea Volcano [abs.], in *Abstract volume*, edited by R. W. Decker, W. T. Wright, and P. H. Stauffer, p. p. 60, U.S. Geol. Surv. Prof. Pap., 1350.
- Eibl, E. P. S., C. J. Bean, K. S. Vogfjörð, Y. Ying, I. Lokmer, M. Möllhoff, G. O’Brien, and F. Palsson (2017), Tremor-rich shallow dyke formation followed by silent magma flow at Bárðarbunga in Iceland, *Nature Geoscience*, doi:10.1038/NGEO2906.
- Falsaperla, S., S. Alparone, S. D’Amico, G. Grazia, F. Ferrari, H. Langer, T. Sgroi, and S. Spampinato (2005), Volcanic tremor at Mt. Etna, Italy, preceding and accompanying the eruption of July - August, 2001, *Pure and Applied Geophysics*, *162*(11), 2111–2132, doi:10.1007/s00024-005-2710-y.
- Flóvenz, Ó. G., and K. Gunnarsson (1991), Seismic crustal structure in Iceland and surrounding area, *Tectonophysics*, *189*(1-4), 1–17, doi:10.1016/0040-1951(91)90483-9.
- Garel, F., E. Kaminski, S. Tait, and A. Limare (2012), An experimental study of the surface thermal signature of hot subaerial isoviscous gravity currents: Implications for thermal monitoring of lava flows and domes, *Journal of Geophysical Research: Solid Earth*, *117*(2), 1–18, doi:10.1029/2011JB008698.
- Harris, A. (2013), *Thermal remote sensing of active volcanoes: a user’s manual*, vol. 100, 736 pp., Cambridge University Press, doi:10.1017/CBO9781139029346.
- Hibert, C., A. Mangeney, M. Polacci, A. D. Muro, S. Vergnolle, V. Ferrazzini, A. Peltier, B. Taisne, M. Burton, T. Dewez, G. Grandjean, A. Dupont, T. Staudacher, F. Brenguier, P. Kowalski, P. Boissier, P. Catherine, and F. Lauret (2015), Toward continuous quantification of lava extrusion rate: Results from the multidisciplinary analysis of the 2 January 2010 eruption of Piton de la Fournaise volcano, la Réunion, *Journal of Geophysical Research B: Solid Earth*, *120*(5), 3026–3047, doi:10.1002/2014JB011769.
- Hjartardóttir, Á. R., P. Einarsson, M. T. Gudmundsson, and T. Högnadóttir (2016), Fracture movements and graben subsidence during the 2014 Bárðarbunga dike intrusion in Iceland, *Journal of Volcanology and Geothermal Research*, *310*, 242–252, doi:10.1016/j.jvolgeores.2015.12.002.
- Hotovec, A. J., S. G. Prejean, J. E. Vidale, and J. Gombert (2013), Strongly gliding harmonic tremor during the 2009 eruption of Redoubt Volcano, *Journal of Volcanology and Geothermal Research*, *259*, 89–99, doi:10.1016/j.jvolgeores.2012.01.001.
- Julian, B. R. (1994), Volcanic tremor: Nonlinear excitation by fluid flow, *Journal of Geophysical Research*, *99*(B6), 11,859–11,877, doi:10.1029/93JB03129.
- Kedar, S., H. Kanamori, and B. Sturtevant (1998), Bubble collapse as the source of tremor at Old Faithful Geyser, *Journal of Geophysical Research*, *103*(B10), 24,283–24,299, doi:10.1029/98JB01824.
- Koyanagi, R. Y., B. A. Chouet, and K. Aki (1987), Origin of volcanic tremor in Hawaii, part I. Data from the Hawaiian Volcano Observatory, 1969–1985, in *U.S. Geological Survey Professional Paper 1350*, vol. v. 2, edited by R. W. Decker, T. W. Wright, and P. H. Stauffer, pp. p. 1221–1257, U.S. Geol. Surv. Prof. Pap., 1350.

- Krüger, F., and M. Weber (1992), The effect of low-velocity sediments on the mislocation vectors of the GRF array, *Geophys. J. Int.*, *108*(1), 387–393, doi:10.1111/j.1365-246X.1992.tb00866.x.
- La Rocca, M., D. Galluzzo, S. Malone, W. McCausland, G. Saccorotti, and E. Del Pezzo (2008), Testing small-aperture array analysis on well-located earthquakes, and application to the location of deep tremor, *Bulletin of the Seismological Society of America*, *98*(2), 620–635, doi:10.1785/0120060185.
- Langer, H., S. Falsaperla, A. Messina, S. Spampinato, and B. Behncke (2011), Detecting imminent eruptive activity at Mt Etna, Italy, in 2007-2008 through pattern classification of volcanic tremor data, *Journal of Volcanology and Geothermal Research*, *200*(1-2), 1–17, doi:10.1016/j.jvolgeores.2010.11.019.
- Leet, R. C. (1988), Saturated and subcooled hydrothermal boiling in groundwater flow channels as a source of harmonic tremor, *Journal of Geophysical Research*, *93*(B5), 4835, doi:10.1029/JB093iB05p04835.
- McNutt, S. R. (1987), Volcanic tremor at Pavlof Volcano, Alaska, October 1973–April 1986, *Pure and Applied Geophysics PAGEOPH*, *125*(6), 1051–1077, doi:10.1007/BF00879368.
- McNutt, S. R. (1992), Volcanic Tremor, *Encyclopedia of Earth System Science*, *4*, 417–425.
- McNutt, S. R. (1994), Volcanic tremor amplitude correlated with eruption explosivity and its potential use in determining ash hazards to aviation, *U.S. Geol. Survey Bull.* *2047*, pp. 377–385.
- Megies, T., M. Beyreuther, R. Barsch, L. Krischer, and J. Wassermann (2011), ObsPy - what can it do for data centers and observatories?, *Annals of Geophysics*, *54*(1), 47–58, doi:10.4401/ag-4838.
- Nadeau, P. A., J. L. Palma, and G. P. Waite (2011), Linking volcanic tremor, degassing, and eruption dynamics via SO₂ imaging, *Geophysical Research Letters*, *38*(1), n/a–n/a, doi:10.1029/2010GL045820.
- Neuberg, J., R. Luckett, B. Baptie, and K. Olsen (2000), Models of tremor and low-frequency earthquake swarms on Montserrat, *Journal of Volcanology and Geothermal Research*, *101*(1-2), 83–104, doi:10.1016/S0377-0273(00)00169-4.
- Palma, J. L., E. S. Calder, D. Basualto, S. Blake, and D. A. Rothery (2008), Correlations between SO₂ flux, seismicity, and outgassing activity at the open vent of Villarrica volcano, Chile, *Journal of Geophysical Research: Solid Earth*, *113*(10), doi:10.1029/2008JB005577.
- Patrick, M. R., T. Orr, D. Wilson, D. Dow, and R. Freeman (2011), Cyclic spattering, seismic tremor, and surface fluctuation within a perched lava channel, Kilauea Volcano, *Bulletin of Volcanology*, *73*(6), 639–653, doi:10.1007/s00445-010-0431-2.
- Pedersen, G., Á. Höskuldsson, T. Thordarson, I. Jónsdóttir, M. S. Riishuus, B. Oskarsson, S. Dumont, E. Magnússon, and M. T. Gudmundsson (2017), Lava field evolution and emplacement dynamics of the Holuhraun 2014-2015 eruption, Iceland., *Journal of Volcanology and Geothermal Research*, *accepted*.
- Pieri, D. C., and S. M. Baloga (1986), Eruption rate, area, and length relationships for some Hawaiian lava flows, *Journal of Volcanology and Geothermal Research*, *30*(1-2), 29–45, doi:10.1016/0377-0273(86)90066-1.
- Ripepe, M., and E. Gordeev (1999), Gas bubble dynamics model for shallow volcanic tremor at Stromboli, *Journal of Geophysical Research*, *104*(B5), 10,639, doi:10.1029/98JB02734.
- Ripepe, M., D. Delle Donne, G. Lacanna, E. Marchetti, and G. Ulivieri (2009), The onset of the 2007 Stromboli effusive eruption recorded by an integrated geophysical network, *Journal of Volcanology and Geothermal Research*, *182*(3-4), 131–136, doi:10.1016/j.jvolgeores.2009.02.011.
- Schweitzer, J. (2001), Slowness corrections - One way to improve IDC products, *Pure and Applied Geophysics*, *158*, 375–396, doi:10.1007/PL00001165.

- Senyukov, S. L., I. N. Nuzhdina, S. Y. Droznina, V. T. Garbuzova, T. Y. Kozhevnikova, O. V. Sobolevskaya, Z. A. Nazarova, and V. E. Bliznetsov (2015), Reprint of "Seismic monitoring of the Plosky Tolbachik eruption in 2012-2013 (Kamchatka Peninsula Russia)", *Journal of Volcanology and Geothermal Research*, *307*, 47–59, doi:10.1016/j.jvolgeores.2015.07.026.
- Sigmundsson, F., A. Hooper, S. Hreinsdóttir, K. S. Vogfjörð, B. G. Ófeigsson, E. R. Heimisson, S. Dumont, M. Parks, K. Spaans, G. B. Gudmundsson, V. Drouin, T. Árnadóttir, K. Jónsdóttir, M. T. Gudmundsson, T. Högnadóttir, H. M. Fridriksdóttir, M. Hensch, P. Einarsson, E. Magnússon, S. Samsonov, B. Brandsdóttir, R. S. White, T. Ágústsdóttir, T. Greenfield, R. G. Green, Á. R. Hjartardóttir, R. Pedersen, R. a. Bennett, H. Geirsson, P. C. La Femina, H. Björnsson, F. Pálsson, E. Sturkell, C. J. Bean, M. Möllhoff, A. K. Braiden, and E. P. S. Eibl (2014), Segmented lateral dyke growth in a rifting event at Bárarbunga volcanic system, Iceland., *Nature*, *517*(7533), 15, doi:10.1038/nature14111.
- Soosalu, H., P. Einarsson, and B. S. Þorbjarnardóttir (2005), Seismic activity related to the 2000 eruption of the Hekla volcano, Iceland, *Bulletin of Volcanology*, *68*(1), 21–36, doi:10.1007/s00445-005-0417-7.
- Tárraga, M., J. Martí, R. Abella, R. Carniel, and C. López (2014), Volcanic tremors: Good indicators of change in plumbing systems during volcanic eruptions, *Journal of Volcanology and Geothermal Research*, *273*, 33–40, doi:10.1016/j.jvolgeores.2014.01.003.
- Thordarson, T., Á. Höskuldsson, I. Jónsdóttir, G. Pedersen, M. T. Gudmundsson, T. Dürig, M. S. Riishuus, W. Moreland, J. Gudnason, C. R. Gallagher, and R. A. Askew (2015), Emplacement and Growth of the August 2014 to February 2015 Nornahraun Lava Flow Field North Iceland, in *Amercian Geophysical Union*.
- Witt, T., and T. R. Walter (2017), Video monitoring reveals pulsating vents and propagation path of fissure eruption during the March 2011 Pu'u " eruption, Kilauea volcano, *Journal of Volcanology and Geothermal Research*, *330*, 43–55, doi:10.1016/j.jvolgeores.2016.11.012.
- Wright, R., S. Blake, A. J. L. Harris, and D. A. Rothery (2001), A simple explanation for the space-based calculation of lava eruption rates, *Earth and Planetary Science Letters*, *192*(2), 223–233, doi:10.1016/S0012-821X(01)00443-5.
- Zhang, J.-Y., Y. Chen, and X.-x. Huang (2009), Edge detection of images based on improved Sobel operator and genetic algorithms, in *2009 International Conference on Image Analysis and Signal Processing*, pp. 31–35, doi:10.1109/IASP.2009.5054605.

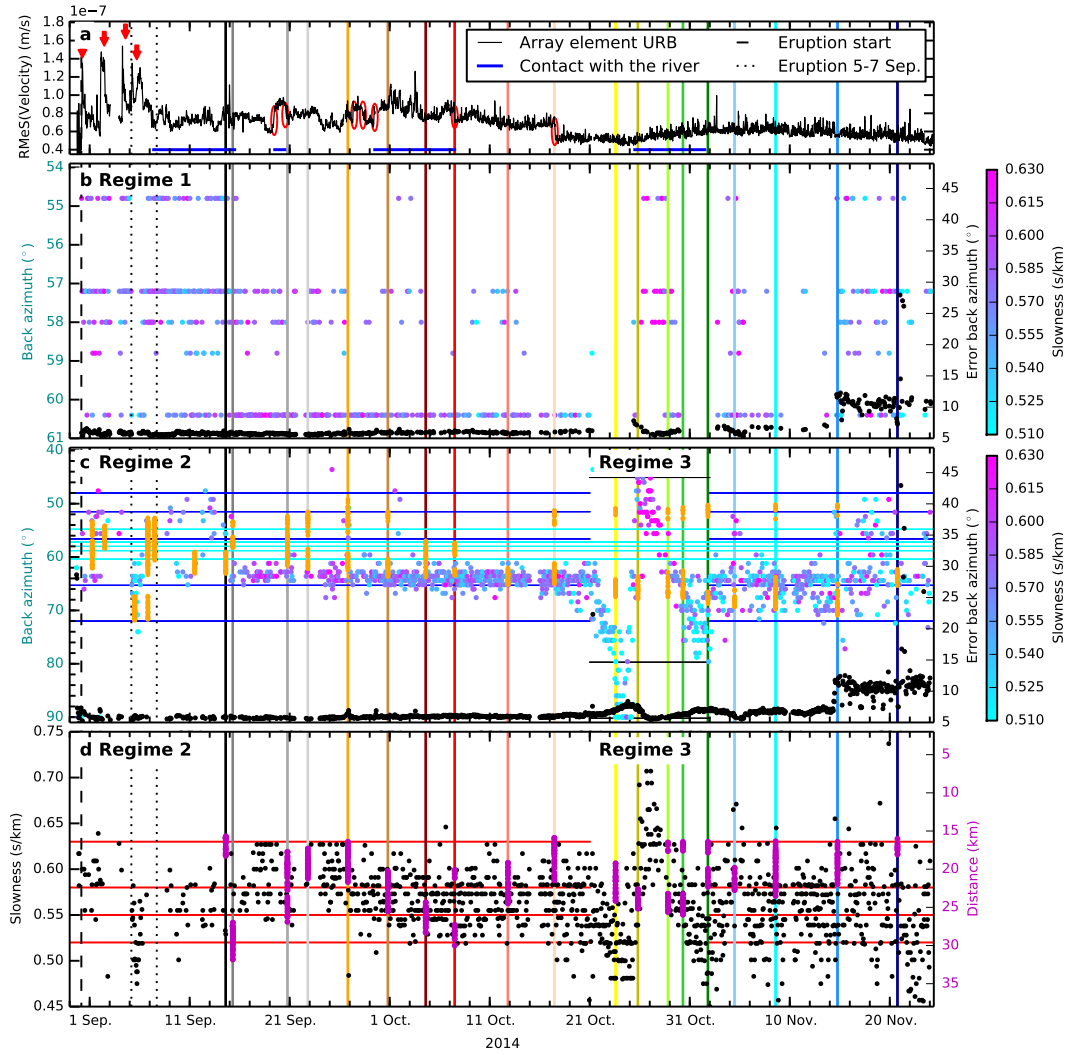


Figure 6. Separation of tremor sources based on the back azimuth between 31 August and 24 November, 2014. (a) RMeS (black), black dashed line and red arrows as in Fig. 5. Red ellipses mark sudden increases or decreases in tremor amplitude and blue horizontal lines mark when the lava flow field flowed into Jökulsá á Fjöllum river. Dotted lines mark the start and end of the eruption on 5-7 September. Colored vertical lines indicate when the lava flow field was mapped with colors corresponding to Fig. 3. (b) Dots colored according to slowness mark each 1 h long time window where one of the five stable back azimuths in Regime 1 is dominating. Black dots indicate the corresponding error of the back azimuth. It increased on 14 November when stations started to fail. Black and colored vertical lines as in a. (c) Dots colored according to slowness mark each 1 h long time window in Regime 2 and 3 where the back azimuth is none of the five stable directions in Regime 1. Black dots as in b, colored and black vertical lines as in a. Orange dots indicate the back azimuth of the actively growing flow front. Cyan horizontal lines mark the five stable directions in Regime 1 and black lines mark the minimum and maximum back azimuth in Regime 3. Blue lines mark the overall northernmost direction, northern and southernmost directions before 15 September, the southernmost direction between 15 September and 21 October and the overall southernmost direction in Regime 2. Projections are shown in Fig. 3. (d) Same as c but for slowness instead of back azimuth marked with black dots. Red horizontal lines mark minimum and maximum slowness observed before 21 October, minimum slowness on 23 September and on 27 September to 1 October and are projected in Fig. 3. Magenta dots mark the distance between the newly formed lava flow field and UR array as visible in Fig. 3.

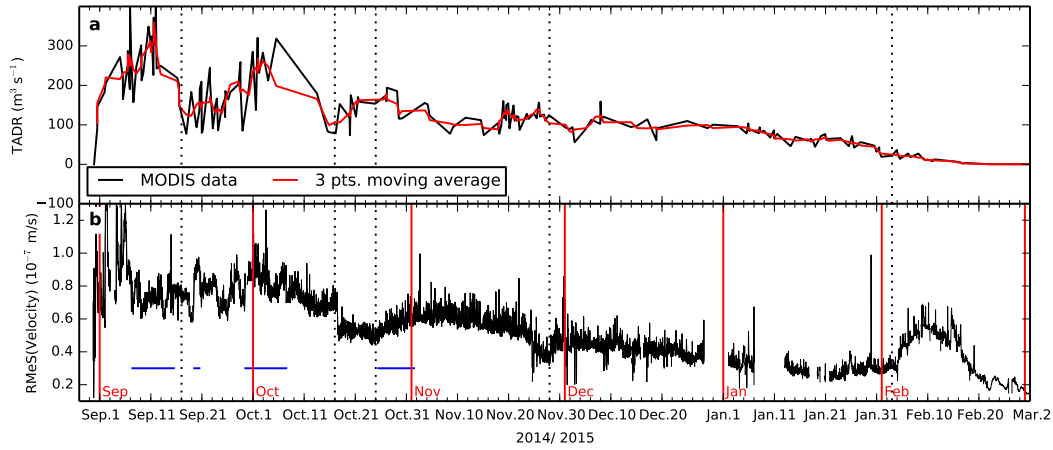


Figure 7. Comparison of RMeS of the tremor with effusion rate from 31 August 2014 to 2 March 2015. Dotted lines are for orientation. (a) MODIS-derived Time Averaged lava Discharge Rate (TADR). (b) RMeS of array station URB (black line). Blue horizontal lines mark times of contact between the growing lava front with Jökulsá á Fjöllum river. Red vertical lines mark the beginning of months.

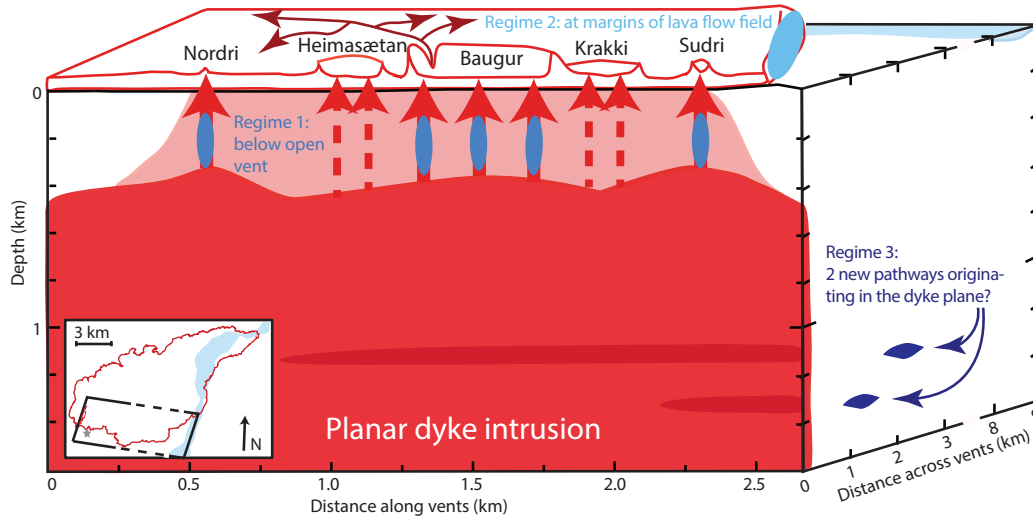


Figure 8. Schematic illustration of the locations of the three tremor Regimes. It was inferred from InSAR, GPS and superficial fault mappings that the tip of the dyke (red plane) was located at a few hundred meters depth beneath the eruptive site on the day before the eruption. In the first 24 h the whole dyke might have reached the surface as indicated by the light red region. The vents that remain open from day 2 are marked with red, solid arrows. Red dashed lines mark regions that fed vents for a few days only and generated no or weak tremor. Light, medium and dark blue regions mark the array located tremor source regions. This is mainly at the margins of the lava flow field (Regime 2), shallow in the open vents (Regime 1) and potentially whilst new intrusions happened (Regime 3). Note that even on the first day tremor is preferably generated in the medium blue regions, and that the dark blue tremor in Regime 3 appears red when it is located behind the planar dyke intrusion. Dark red arrows indicate the main feeding system in the lava flow field. The inset indicates the illustrated part of the lava flow field and vent area where the grey star marks the location of oblique superficial fractures (pers. comm. Ásta Rut Hjartardóttir, December 2016).